10th International Conference
12-14 July 2010
Southampton
RASD 2010

ALTERNATIVE MODAL BASIS SELECTION PROCEDURES FOR NONLINEAR RANDOM RESPONSE SIMULATION

Adam Przekop[1*], Xinyun Guo[2] and Stephen A. Rizzi[3]

[1]Analytical Services and Materials, Inc.
107 Research Dr.
Hampton, Virginia 23666 USA
E-mail: Adam.Przekop@nasa.gov

[2]School of Engineering and Computer Science
Daniel Webster College
Nashua, New Hampshire 03063 USA
E-mail: Guo_David@dwc.edu

[3]NASA Langley Research Center
Structural Acoustics Branch
Hampton, Virginia 23681 USA
E-mail: Stephen.A.Rizzi@nasa.gov

Keywords: Random response identification, Nonlinear reduced-order simulation.

ABSTRACT

Three procedures to guide selection of an efficient modal basis in a nonlinear random response analysis are examined. One method is based only on proper orthogonal decomposition, while the other two additionally involve smooth orthogonal decomposition. Acoustic random response problems are employed to assess the performance of the three modal basis selection approaches. A thermally post-buckled beam exhibiting snap-through behavior, a shallowly curved arch in the auto-parametric response regime and a plate structure are used as numerical test articles. The results of the three reduced-order analyses are compared with the results of the computationally taxing simulation in the physical degrees of freedom. For the cases considered, all three methods are shown to produce modal bases resulting in accurate and computationally efficient reduced-order nonlinear simulations.

LIST OF ACRONYMS

DoF	Degree-of-freedom
LNM	Linear normal mode
MAP	Modal amplitude participation
POD	Proper orthogonal decomposition
POV	Proper orthogonal value
SOD	Smooth orthogonal decomposition
EPF	Estimated POM frequency
MAC	Modal assurance criterion
MEP	Modal energy participation
POM	Proper orthogonal mode
SOM	Smooth orthogonal mode
SOV	Smooth orthogonal value

1. INTRODUCTION

Nonlinear random response analysis of large structural components in physical degrees of freedom (DoFs) can be associated with a prohibitive computational cost. Reduced-order modeling has been shown to be a viable alternative for a range of loading and response conditions [1-8]. For a typical aerospace structure having complex geometry and loading conditions (combined mechanical, thermal, acoustic, and pressure), selection of basis functions through which the reduced-order system is formed is usually not intuitive. Therefore, a rigorous modal basis selection procedure resulting in a computationally efficient and accurate reduced-order simulation is required. As part of that procedure, a system identification procedure must be performed and a criterion for modal basis selection must be established.

Recently, Rizzi and Przekop offered a modal basis procedure and successfully demonstrated it on 1-D and 2-D thin-walled structures [9-11]. Because the identification procedure utilized displacement response data in a proper orthogonal decomposition (POD) analysis, the modal basis selection criterion relied solely on proper orthogonal mode (POM) amplitudes. However, different DoF types (e.g. transverse or in-plane displacements) often times exhibit significantly different response magnitudes, so the selection process had to be performed independently for each DoF type to avoid discriminating against important response components having small amplitudes. This procedure for selecting POMs is subsequently referred to as the *modal amplitude participation* (MAP) procedure. Finally, since POMs are load dependent, linear normal modes (LNMs) were related to the POMs to form a robust, load independent modal basis.

A modified approach to mitigate the need to process individual DoFs types separately in the basis selection process was subsequently presented by Guo and Przekop [12]. It additionally included velocity response data in the identification process by means of the smooth orthogonal decomposition (SOD) analysis [13]. Through this enhancement, estimated frequencies corresponding to POMs became available. This permitted a measure of the modal energy corresponding to a particular POM to be computed and used in the selection process. The process through which modal energy is used for selecting POMs is subsequently referred to as the *modal energy participation* (MEP) procedure. Consequently, in the MEP approach, different DoF types were handled together and small displacement amplitude responses were not discriminated against if their corresponding energy was high. The MEP procedure was successfully tested by comparing the reduced-order analysis results with those obtained from full-order simulations in physical DoFs. However, since the MAP procedure was tested using a general reduced-order approach retaining all the DoFs [9-11], and the MEP procedure was tested using a reduced-order method variation that statically condenses the in-plane behavior into transverse equations [12], a direct comparison of the effectiveness of the two procedures was not possible. Introduction of the SOD enhancement to the identification process enabled one additional alternative for modal basis selection not previously considered. The approach retains POMs within some specified frequency bandwidth based on their *estimated POM frequencies* (EPF). As in the MAP approach, LNMs are used to form the basis from the selected POMs in both the MEP and EPF approaches.

The objectives of this study are twofold. The first is to evaluate the modal bases derived using the MAP, MEP and EPF approaches. The second is to compare reduced-order analysis results, obtained with the same reduced-order approach, using the three different bases with results from a full-order simulation. The 1-D and 2-D structures previously investigated [9-11] will serve as the example cases.

2. FORMULATION

In this section, the three components required for an accurate and computationally efficient reduced-order analysis are outlined. They are system identification, modal basis selection, and nonlinear modal reduction and simulation.

2.1 System identification

When physical DoFs are chosen to characterize a response, two data sets can be formed as an accumulation of n instantaneous displacement and velocity fields to produce a displacement snapshot matrix $\mathbf{X}$ and a velocity snapshot matrix $\mathbf{V}$, respectively. Both matrices contain the same selected set of N DoFs resulting in their sizes being $n \times N$. The sample rate and spatial resolution of the snapshot matrices must be sufficient to resolve the system's temporal and spatial characteristics of interest. The displacement and velocity correlation matrices $\mathbf{R}_{\mathrm{X}}$ and $\mathbf{R}_{\mathbf{V}}$, respectively, both of size $N \times N$ are formed as

$$\mathbf{R}_{\mathbf{X}} = \frac{1}{n}\mathbf{X}^{\mathrm{T}}\mathbf{X} \tag{1}$$

and

$$\mathbf{R}_{\mathbf{V}} = \frac{1}{n}\mathbf{V}^{\mathrm{T}}\mathbf{V} . \tag{2}$$

An eigenanalysis of the displacement correlation matrix $\mathbf{R}_{\mathrm{X}}$ is next performed, i.e.,

$$\left[\mathbf{R}_{\mathbf{X}} - \lambda\mathbf{I}\right]\mathbf{p} = \mathbf{0} \tag{3}$$

to obtain the POM matrix $\mathbf{P} = \left[\mathbf{p}_1\ \mathbf{p}_2\ \ldots\ \mathbf{p}_N\right]$ and the diagonal proper orthogonal value (POV) matrix, $\boldsymbol{\lambda}$, both of size $N \times N$ [14]. Note that an alternative means of obtaining similar quantities is via singular value decomposition [15]. Another eigenanalysis can be performed to obtain the smooth orthogonal mode (SOM) matrix $\mathbf{S} = \left[\mathbf{s}_1\ \mathbf{s}_2\ \ldots\ \mathbf{s}_N\right]$ and the diagonal smooth orthogonal value (SOV) matrix, $\boldsymbol{\gamma}$, both of size $N \times N$ [13]

$$\left[\mathbf{R}_{\mathbf{V}} - \gamma\mathbf{R}_{\mathbf{X}}\right]\mathbf{s} = \mathbf{0} . \tag{4}$$

Here the smooth orthogonal values $\boldsymbol{\gamma}$ are the squared natural frequencies of the SOMs. Solution of the eigenanalysis (4), however, does not directly give the sought after estimated POM frequencies. Chelidze and Zhou [13] and Farooq and Feeny [16] independently showed that natural frequencies corresponding to the j-th SOM can also be estimated from a Rayleigh quotient-like relationship as

$$\gamma_j = \omega_j^2 = \frac{\mathbf{s}_j^{\mathrm{T}}\mathbf{R}_{\mathbf{V}}\mathbf{s}_j}{\mathbf{s}_j^{\mathrm{T}}\mathbf{R}_{\mathbf{X}}\mathbf{s}_j} . \tag{5}$$

They further showed that for an undamped linear free vibration problem

$$\mathbf{\Phi} = \mathbf{S}^{-\mathbf{T}} \tag{6}$$

where $\mathbf{\Phi}$ is a linear modal matrix. Since any vibrating system, even a nonlinear one, can be expressed as a superposition of POMs **p**, Eq. (6) can be used to make the following approximation

$$\mathbf{S} \cong \mathbf{P}^{-\mathbf{T}} \ . \tag{7}$$

Substitution of Eq. (7) into Eq. (5) is performed to obtain the desired estimated POM frequencies, without the need of solving Eq. (4) directly.

2.2 Modal basis selection

Three approaches (MAP, MEP and EPF) are offered for selecting the basis required in the reduced-order analysis. In each approach, a set of POMs is first identified followed by a procedure to associate each POM with one or more LNMs. The EPF approach uses Eqs. (5) and (7) to select a set of POMs within some desired frequency band. The MAP selects POMs using a modal amplitude participation factor [9-11], while the MEP approach uses a modal energy participation factor as described below.

Feeny and Liang [17] showed that for lightly damped randomly excited systems and large but finite number of simulation time steps *n*, the POVs approximate the mean square values of modal coordinates, *q*, i.e.,

$$\lambda_j = \frac{1}{n}\sum_{i=1}^{n}\left(q_i^j\right)^2 \ . \tag{8}$$

Note that the number of simulation time steps is typically greater than the number of time steps used in the correlation matrices for system identification. Assume that a measure of the instantaneous modal kinetic energy associated with the *j*-th POM can be represented as

$$e_i^j \cong \omega_j^2\left(q_i^j\right)^2 \ . \tag{9}$$

The mean modal kinetic energy over *n* simulation time steps becomes

$$\overline{e}_j \cong \frac{1}{n}\sum_{i=1}^{n} e_i^j \ . \tag{10}$$

Substituting Eq. (9) into Eq. (10) yields

$$\overline{e}_j \cong \omega_j^2 \frac{1}{n}\sum_{i=1}^{n}\left(q_i^j\right)^2 \ . \tag{11}$$

Further substituting Eqs. (5) and (8) into Eq. (11) yields the mean modal kinetic energy in terms of the POVs and their estimated squared frequencies as

$$\overline{e}_j \cong \gamma_j \lambda_j \ . \tag{12}$$

The contribution of each POM to the overall dynamic response is given by

$$\chi_j = \frac{\overline{e}_j}{\sum_{j=1}^{N} \overline{e}_j} \qquad j = 1, \ldots, N \tag{13}$$

where χ_j is the *j*-th POM modal energy participation factor. The sum of all POM modal energy participation factors is unity. When the dominant *M* POMs are selected, their cumulative participation, υ, can be expressed as

$$\upsilon = \sum_{j=1}^{M} \chi_j \qquad 0 < \upsilon \leq 1 \ . \tag{14}$$

Retention of only *M* selected POMs reduces the size of **P** to *M* x *N*. Note that Eqs. (13) and (14) can be also used to obtain the MAP approaches' modal amplitude participation factor and cumulative participation [9-11], respectively, when the POVs λ_j are used in place of the mean modal kinetic energy. Unlike the MEP approach which requires only a single criterion for either Eq. (13) of (14), the MAP approach requires as many criteria as there are DoF types used in the system identification, e.g. one cutoff value for the transverse displacement and one value for the in-plane displacement. For both the MAP or MEP approaches, a set of POMs may be selected based on the modal participation factor, the cumulative participation, or some combination thereof.

The final step in the modal basis selection process follows the selection of POMs via one or more of the above approaches. As previously indicated, the direct use of POMs as the basis functions is not preferred as they are specific to the loading under which they were determined and, consequently, applicability of such a basis to alternative loading conditions may be limited. Instead, a more robust load-independent basis, formed from LNMs **Φ** which resemble the *M* selected POMs, is sought. To do so, the expansion coefficient matrix $\mathbf{C}_{\mathbf{exp}}$ is first produced by crossing the transpose of the LNM matrix and the matrix of the selected POMs

$$\mathbf{C}_{\mathbf{exp}} \cong \mathbf{\Phi}^{-\mathrm{T}}\mathbf{P} \ . \tag{15}$$

Each column of $\mathbf{C}_{\mathbf{exp}}$ corresponds to a particular POM and provides the coefficients required for LNM superposition. Since the POMs are not normalized, each column of coefficients is individually normalized such that its maximum value is unity. In this manner, a single cut-off value can be specified for all POMs. The cut-off value selection is arbitrary, but previous experience proved that a value of 0.5 gives reasonable results [9-10]. The end result of the basis selection process is a set of *L* selected LNMs, $L \ll N$, for use in the nonlinear modal reduction. Note, that an alternative approach for correlating the selected POMs with the LNMs utilizing the modal assurance criterion (MAC) was explored by the authors in the past [11].

2.3 Nonlinear modal reduction and simulation

Since the modal reduction utilizing the indirect approach employing a nonlinear stiffness evaluation procedure was detailed by the authors in several recent publications [1, 9-11, 18], only an abbreviated description is presented herein. The equations of motion of the nonlinear full-order system in physical DoFs may be written as

$$\mathbf{M}\ddot{\mathbf{x}}(t)+\mathbf{C}\dot{\mathbf{x}}(t)+\mathbf{f}_{\mathbf{NL}}(\mathbf{x}(t))=\mathbf{f}(t) \tag{16}$$

where **M** and **C** are the system mass and damping matrices, **x** is the displacement response vector and **f** is the force excitation vector, respectively. The nonlinear restoring force $\mathbf{f}_{\mathbf{NL}}$ is a vector function, which generally includes the linear, quadratic, and cubic stiffness terms. By applying the modal coordinate transformation

$$\mathbf{x}(t)=\mathbf{\Phi}\mathbf{q}(t) \tag{17}$$

to Eq. (16), a modal equation of motion can be written as

$$\tilde{\mathbf{M}}\ddot{\mathbf{q}}(t)+\tilde{\mathbf{C}}\dot{\mathbf{q}}(t)+\tilde{\mathbf{f}}_{\mathbf{NL}}(\mathbf{q}_1(t),\mathbf{q}_2(t),\ldots,\mathbf{q}_L(t))=\tilde{\mathbf{f}}(t) \tag{18}$$

where $\mathbf{q}=[q_1,q_2,\ldots,q_L]^{\mathrm{T}}$ is a generalized coordinate vector and $\mathbf{\Phi}$ is the set of L selected LNMs. For mass-normalized eigenvectors,

$$\tilde{\mathbf{M}}=\mathbf{\Phi}^{\mathrm{T}}\mathbf{M}\mathbf{\Phi}=\lceil\mathbf{I}\rfloor \qquad \tilde{\mathbf{C}}=\mathbf{\Phi}^{\mathrm{T}}\mathbf{C}\mathbf{\Phi}=\lceil 2\zeta_r\omega_r\rfloor \tag{19}$$

and ω_r are the undamped natural frequencies and ζ_r are the viscous damping factors. The modal excitation force is $\tilde{\mathbf{f}}=\mathbf{\Phi}^{\mathrm{T}}\mathbf{f}$.

Since the nonlinear restoring force $\mathbf{f}_{\mathbf{NL}}$ is generally not known in the context of a commercial finite element (FE) program, an indirect means of evaluating the nonlinear stiffness is required. Different combinations of scaled LNMs can be used to form a set of prescribed displacement fields. Using a nonlinear FE static analysis, nonlinear restoring forces $\mathbf{f}_{\mathbf{NL}}$ can be computed in physical DoFs and transformed to the generalized coordinates as $\tilde{\mathbf{f}}_{\mathbf{NL}}=\mathbf{\Phi}^{\mathrm{T}}\mathbf{f}_{\mathbf{NL}}$. The r-th nonlinear modal restoring force can be written as a summation of modal linear, quadratic, and cubic stiffness components as

$$\tilde{f}^r_{NL}(q_1,q_2,\ldots,q_L)=\sum_{j=1}^{L}d^r_j q_j+\sum_{j=1}^{L}\sum_{k=j}^{L}a^r_{jk}q_j q_k+\sum_{j=1}^{L}\sum_{k=j}^{L}\sum_{l=k}^{L}b^r_{jkl}q_j q_k q_l \qquad r=1,2,\ldots,L \tag{20}$$

Since the left-hand-side of the Eq. (20) is known, as are the assumed scaling factors q on its right-hand-side, solution of a simple algebraic system of equations is only needed to arrive at the linear d, quadratic a, and cubic b modal stiffness coefficients. Eq. (18) is numerically integrated using a 4th order Runge-Kutta scheme and physical displacements are obtained through the inverse modal coordinate transform.

3. APPLICATION EXAMPLES

The beam, arch, and plate structures previously considered [9-11] serve as example cases. Identified POMs, their corresponding frequencies, modal energy participation factors, and results of POM projections on a set of LNMs are used to compare the three modal basis selection methods. Transverse and in-plane displacement power spectral densities (PSDs) are used to assess the quality of the resulting reduced-order simulations vis-à-vis full-order

simulations. ABAQUS/Explicit v6.9 [19] and the ABAQUS-based RANSTEP code [18] were used in the study to produce full-order and reduced-order solutions, respectively.

3.1 Beam example

The aluminum planar beam structure employed in this study is the same as previously investigated by the authors [11]. The following material properties were used: Young's modulus E = 73.11 GPa, shear modulus G = 27.59 GPa, mass density ρ = 2763 kg/m^3, and coefficient of thermal expansion $\alpha = 22.32 \times 10^{-6}$ 1/ºC. A 2% critical damping, corresponding to the first symmetric transverse displacement LNM, was prescribed. The beam measured 0.4572 m in length with a cross-section of 25.4 mm wide by 2.286 mm high. The FE beam model was discretized using 144 ABAQUS two node B21 elements, each measuring 3.175 mm in length. The B21 element features three DoFs per node; one rotational DoF and two translational (transverse and in-plane) DoFs. Hence the beam FE model contained a total of 435 DoFs. Both beam ends were clamped, i.e., all three DoFs at the two end nodes were constrained.

The random load was modeled as truncated white noise [20] with the cut-off frequency of 1500 Hz. The loading had an overall sound pressure level (OASPL) of 170 dB referenced to 20 μPa. In addition, a uniform temperature increment of 19.44 ºC was applied. This temperature increment was approximately 5.3 times the critical buckling temperature of 3.67 ºC and resulted in two symmetric thermally post-buckled equilibrium positions. Since the temperature increase was relatively small, the material properties were considered to be temperature-independent. Under the prescribed combination of temperature and acoustic loadings, the beam was known to respond in a persistent snap-through fashion [11].

The total duration of the simulation used to perform the system identification was 2.1384 s from which the initial transient of 0.5 s was removed to ensure that a developed response was applied in the procedure. With the sampling rate at 50 μs, 32,768-point displacement and velocity snapshots were used. The reduced-order simulation results that follow utilize five ensemble averages, giving a total response duration of 8.192 s after removal of the initial transients from each ensemble. A 32,768-point fast Fourier transform (FFT) was used to compute the response PSDs, giving a frequency resolution of 0.61 Hz.

Based on the previous studies conducted using the MAP approach and LNMs identification using MAC values of 0.5 or greater, 17 LNMs were found sufficient to accurately capture the beam response [11]. Therefore, to ensure a meaningful comparison of the results from the three methods, 17 LNMs were also selected using the MEP and EPF procedures. Had the intent of this study been other than to compare the three modal selection procedures, a different criterion could have been used. For example, a certain cumulative participation cut-off level can be established for the MEP approach. Similarly, for the EPF method, a certain cut-off bandwidth can be prescribed.

3.1.1 Beam example results

In the following, the snapshot and correlation matrices were formed using the two translational DoF types only. Section 3.1.1.1 considers the effect of adding the rotational DoF type. The results of the system identification and basis selection processes using the MEP and the EPF methods are presented in Table 1. POM ordering numbers, their corresponding frequencies, modal energy participation factors, and identified LNMs are indicated. While the total set of linear modal basis includes 429 vectors, i.e., the number of active DoFs in the system, the POMs were projected only on a subset of the first 84 LNMs present below 100 kHz. The 17 entries in Table 1 above the dashed red line correspond to the selection of

POMs and their corresponding LNMs using the MEP method. The 17 shaded entries correspond to the POMs and LNMs determined by the EPF method. It is seen that the difference between the two approaches is relatively minor, with LNMs 8 and 9 selected by the MEP method being replaced with LNMs 54 and 58 selected by the EPF method.

The results of the two new procedures are summarized and compared with the original MAP approach in Table 2. Here a breakdown is provided between low frequency transverse LNMs and high frequency in-plane LNMs. It is seen that the EPF and MAP procedures result in the same basis selection.

POM Number	Estimated Frequency, Hz	Modal Energy Participation, %	Identified LNM
290	111.5	45.49	1
289	204.9	16.84	2
288	358.0	15.42	3
286	799.4	8.86	5
287	532.5	7.76	4
284	1440	2.54	7
285	1103	2.35	6
281	1816	0.31	8
280	2246	0.29	9
283	427.0	0.060	15
282	514.2	0.028	22
279	632.5	0.011	28
278	545.0	0.008	33
277	622.1	0.0033	38
276	651.0	0.0027	42
273	904.5	0.0015	47
275	714.5	0.0012	51
271	1107	0.00058	58
270	1245	0.00045	54

Table 1. Selected POMs, their estimated frequencies, modal participation factors, and corresponding LNMs for a beam structure under combined 19.44 ºC and 170 dB loading.

Transverse LNMs					In-plane LNMs				
LNM Number	Frequency (Hz)	MAP (7T + 10I)*	EPF (7T + 10I)	MEP (9T + 8I)	LNM Number	Frequency (Hz)	MAP (7T + 10I)	EPF (7T + 10I)	MEP (9T + 8I)
1	57.82	+	+	+	15	5,625	+	+	+
2	159.34	+	+	+	22	11,250	+	+	+
3	312.29	+	+	+	28	16,874	+	+	+
4	516.05	+	+	+	33	22,495	+	+	+
5	770.56	+	+	+	38	28,114	+	+	+
6	1075.7	+	+	+	42	33,729	+	+	+
7	1431.3	+	+	+	47	39,340	+	+	+
8	1837.3			+	51	44,947	+	+	+
9	2293.3			+	54	50,548	+	+	
* Number of transverse (T) and in-plane (I) LNMs					58	56,144	+	+	

Table 2. Selected eigenanalysis and basis selection results for a beam structure under combined 19.44 ºC and 170 dB loading.

The results of the reduced-order simulations obtained with the three selection procedures as well as the results of the full-order simulation are presented in Figure 1 and Figure 2 for transverse and in-plane displacements, respectively. It is seen that both reduced-order

solutions compare very favorably with the full-order solution and that no particular reduced-order solution seems to provide a more accurate result than the other.

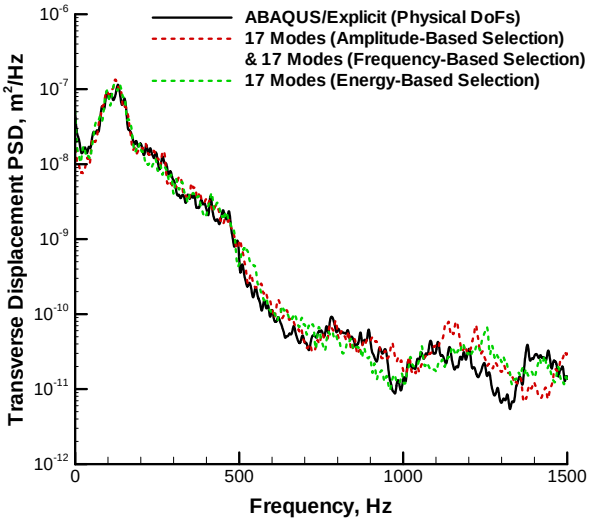

Figure 1. Transverse displacement PSD at the quarter span location.

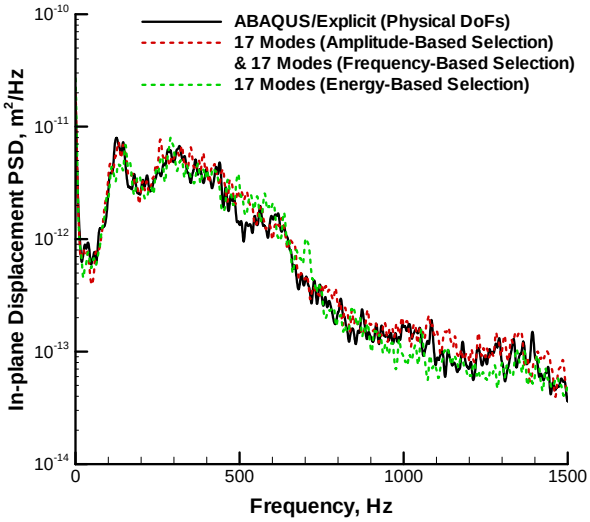

Figure 2. In-plane displacement PSD at the quarter span location.

3.1.1.1 Expanded input degrees-of-freedom

In general, several factors may influence the choice of DoF types which are included in the basis selection procedure. In the preceding section, only two of three element DoF types, namely the translational DoF types, were included in the correlation matrices because this subset of DoF types was proven sufficient in the MAP approach [9-11]. To verify this observation for the two new procedures, the basis selection was repeated using correlation matrices consisting of all three (two translational and one rotational) DoF types. Irrespective of the number of DoF types included in the correlation matrices, the POMs themselves always consist of all three DoF types.

A comparison of POM shapes and estimated frequencies is first presented. The two POMs with the largest modal energy participation factors, POM numbers 290 and 289, were computed using correlation matrices consisting of two and three DoF types. These POMS have the lowest estimated frequencies and are presented in Figure 3 and Figure 4. It is seen that both transverse and in-plane displacement fields match well and also that the frequency estimates are within 10% of each other.

Because the reduced-order analysis uses LNMs as the basis and not POMs directly, the effect of the additional DoF type on the set of LNMs identified is next considered. The inclusion of all three DoF types in the correlation matrices increases the total number of POMs from 290 to 435. As shown in Table 3 for the EPF approach, this increase does not change the number of POMs in the examined low frequency bandwidth and only slightly affects their ordering (compare the frequency ordering of POM numbers 283 and 282 versus POM numbers 422 and 420). However, while the corresponding LNMs were largely unaffected, two POMs (410 and 407) were sufficiently changed such that the number of LNMs identified with each increased from 1 to 2. This would increase the size of the modal basis by 1 (LNM 62) if the frequency bandwidth were to remain fixed. Alternatively, keeping the size of the modal basis fixed at 17 would drop LNM 7 associated with POM number 429.

With regard to the MEP method, inclusion of three DoF types resulted in a basis very similar (1-9, 15, 22, 28, 33, 38, 42, 47, and 54) to that obtained with two DoF types. Only one LNM differed, namely LNM 51 versus 54. This is not surprising as the modal energy

participation factors associated with the POMs are extremely low, 0.0012 and 0.00045%, see Table 1. When the modal energy participation factors are so low, small differences in the POM ordering are not unexpected. In summary, it may be concluded that POM shapes and frequency estimates are not significantly affected by the addition of the rotational DoF type in the correlation matrices, and that any such differences have a minor effect on the derived modal basis. From a practical standpoint, it allows all DoF types to be used in the correlation matrices without the burden of partitioning the snapshot matrices.

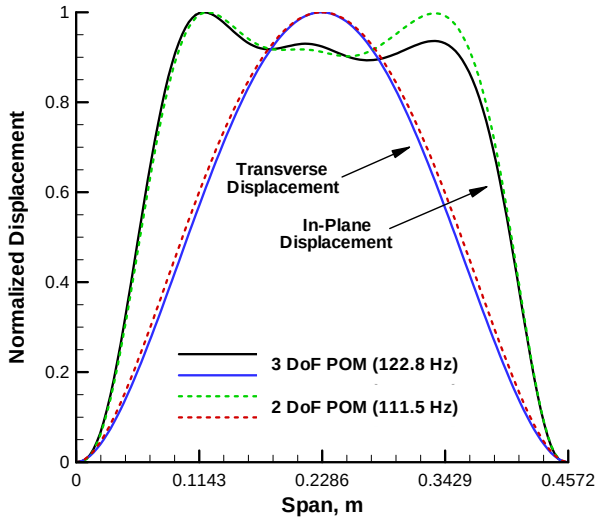

Figure 3. POM number 290 – transverse and in-plane normalized displacements.

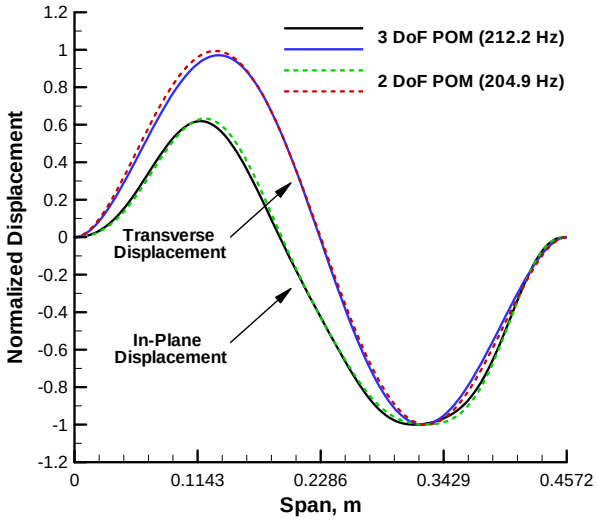

Figure 4. POM number 289 – transverse and in-plane normalized displacements.

3.1.1.2 Comparison of estimated POM and natural frequencies

Additional insight into the relationship between POMs and LNMs can be made through examination of the estimated POM frequencies and LNM frequencies in Table 3. In the following, the results from only the two DoF type identification procedure will be considered for brevity. For the transverse behavior, the range of the estimated POM frequencies (111.5-1440 Hz) is comparable to the range of frequencies for the corresponding LNM frequencies 1-7. Since the response is nonlinear, it is expected that estimated POM frequencies will be different than the LNM frequencies obtained from a stress-free eigenanalysis. It is observed, for example, that POM number 290 has an estimated frequency of 111.5 Hz while the corresponding fundamental LNM occurs at the frequency of 57.78 Hz. The 93.0% increase of the estimated POM frequency over the fundamental is indicative of a spring-hardening type of nonlinearity. This nonlinear behavior is also evident in the transverse displacement PSD in Figure 1, which shows the frequency of the dominant peak to be that of POM number 290, the dominant modal energy contributor, see Table 1. It is also noted in Table 3 that the relative difference between the estimated POM frequency and the corresponding LNM frequency diminishes with increasing frequency. For example, the estimated frequency of POM number 289 is only 28.7% greater than the LNM 2 frequency. For POM number 288 and LNM 3, this difference further diminishes to 14.7%, while the highest frequency transverse LNM number 7 virtually matches the frequency of its corresponding POM number 284.

Significantly different conclusions are drawn based on the in-plane behavior. It is seen that while the natural frequencies of the in-plane LNMs presented in Table 3 range from 5.62 kHz (LNM 15) to 56.1 kHz (LNM 58), the corresponding POMs have estimated frequencies between 427.0 Hz and 1245 Hz, i.e., one to two orders of magnitude lower. The

physical significance of this observation is that the in-plane LNMs are indirectly excited through their nonlinear coupling with the transverse LNMs. From the analysis procedure perspective, however, this is of no significance because the modal expansion procedure that associates LNMs with POMs is a curve fitting process that does not take into account modal frequencies. Hence, because the frequency of the associated LNM may be much higher than its estimated POM frequency, the eigenanalysis identifying LNMs must be conducted for a greater frequency range than the estimated POM frequency range.

2 DoF Types		3 DoF Types		LNM	
POM Number	**Estimated Frequency (Hz)**	**POM Number**	**Estimated Frequency (Hz)**	**Number** * Associated With 3 DoF Type Only	**Frequency (HZ)**
290	111.5	435	122.8	1	57.78
289	204.9	434	212.2	2	159.2
288	358.0	433	369.3	3	312.1
283	427.0	422	498.9	15	5,621
282	514.2	420	486.0	22	11,243
287	532.5	432	534.2	4	515.7
278	545.0	417	561.2	33	22,480
277	622.1	418	613.9	28	16,862
279	632.5	415	623.9	38	28,095
276	651.0	414	651.3	42	33,706
275	714.5	411	718.1	51	44,917
286	799.4	431	799.5	5	770.0
273	904.5	410	905.0	47 (54*)	39,314 (50,514*)
285	1103	430	1103	6	1075
271	1107	409	1158	58	56,106
270	1245	407	1372	54 (62*)	50,514 (61,691*)
284	1440	429	1440	7	1430

Table 3. Comparison of the EPF selection procedure using 2 and 3 DoF types.

3.2 Arch example

The shallowly curved arch structure employed in this study was the same as previously studied by the authors [11]. The same aluminum material properties used in the beam study case were applied, including 2% critical damping coefficient corresponding to the first symmetric LNM. The projected length and the cross section dimensions of the arch matched the dimensions of the beam. A constant radius of arch curvature was 2.06 m. The same element size and type, as well as the boundary conditions, were used in the arch FE model as the beam. The random load was again modeled as a truncated white noise with the cut-off frequency of 1500 Hz. The loading was applied as a distributed vertical force with a root-mean-square (RMS) magnitude of 114.3 N/m. Under the prescribed excitation, the arch is known to respond in an auto-parametric fashion [11]. The total duration of the simulation used to perform the system identification and to produce displacement PSD results matched the values used in the beam study case. Based on the previous studies conducted using the MAP approach and LNMs identification using MAC values of 0.5 or greater, 13 LNMs were found sufficient to accurately capture the arch response [11]. Therefore, 13 LNMs were also selected through the MEP and EPF procedures to ensure a meaningful comparison of results.

3.2.1 Arch example results

In the following, the snapshot and correlation matrices were again formed using the two translational DoF types only. The results of the system identification and basis selection process through the MEP and the EPF methods are presented in Table 4. POMs ordering numbers, their corresponding frequencies, modal energy participation factors, and identified LNMs are indicated. While the total set of LNMs includes 429 vectors, the POMs were projected only on a subset of the first 84 LNMs present below 100 kHz. The entries in Table 4 above the dashed red line correspond to the selection of POMs and their corresponding LNMs resulting from the MEP procedure. The shaded entries correspond to the POMs and LNMs determined by the EPF approach. It is seen that the difference between the two approaches are more significant than for the beam case previously discussed. Table 4 also shows that the identified POMs do not resemble LNMs as closely as was observed in the beam case, as several POMs are represented by more than one LNM. Specifically note that POM number 277 is represented by four LNMs. Since only 13 LNMs are to be included in the solution, only the most closely correlated LNM with POM number 277, i.e., LNM 51, was included. LNMs 11, 33, 42, and all modes below the dashed red line were not included in the MEP reduced-order system.

POM Number	Estimated Frequency, Hz	Modal Energy Participation, %	Identified LNMs
290	334.0	41.43	2, 3
288	273.0	21.58	2
287	769.6	20.06	5
289	191.4	11.10	1
285	1408	3.60	7
286	505.2	2.13	4
284	942.1	0.07	6
281	1667	0.02	9, 22
282	865.0	0.01	9, 22
283	588.5	0.007	15
280	1376	0.0033	8
278	1015	0.00078	28
277	1155	0.00064	11, 33, 42, 51
279	506.9	0.00039	33, 42
276	718.0	0.00019	38
275	800.7	0.00015	33, 42, 51, 58
272	799.0	0.00006	58

Table 4. Selected POMs, their estimated frequencies, modal participation factors, and corresponding LNMs for a shallow arch under 114.3 N/m distributed loading.

The breakdown of selected LNMs by DoF type (transverse and in-plane) is provided in Table 5 for the three basis selection methods. Here the in-plane DoF type is defined in curvilinear coordinates. Consistent with the beam example, it is seen that the MEP approach tends to favor more transverse and fewer in-plane LNMs in the basis compared to the other two approaches. As in the beam example, the number of transverse LNMs and the number of in-plane LNMs are the same for the MAP and EPF approaches. Of those numbers, the two approaches differ by only one transverse LNM and one in-plane LNM.

Results from the reduced-order simulations obtained with the three selection procedures and those from the full-order are presented in Figure 5 and Figure 6 for transverse and in-plane displacements, respectively. It is seen that all three reduced-order solutions compare very favorably with the full-order solution. No particular reduced-order solution seems to

provide appreciably more accurate results than the other. Because the EPF procedure does not include LNM 6 in its basis, it fails to capture the third peak in the transverse displacement PSD (Figure 5). This is an artifact of restricting the number of LNMs to 13. Had the criterion for the EPF procedure been to include all POMs within the excitation bandwidth, then LNM 6 would have been included in the basis.

Transverse LNMs					In-plane LNMs				
LNM Number	Frequency (Hz)	MAP (6T + 7I)	EPF (6T + 7I)	MEP (9T + 4I)	LNM Number	Frequency (Hz)	MAP (6T + 7I)	EPF (6T + 7I)	MEP (9T + 4I)
1	158.25	+	+	+	15	5,624	+	+	+
2	258.17	+	+	+	22	11,225	+	+	+
3	400.41	+	+	+	28	16,831	+		+
4	513.19	+	+	+	33	22,437	+	+	
5	773.72	+	+	+	38	28,039	+	+	
6	1070.1			+	42	33,638	+	+	
7	1426.0	+		+	51	44,826	+	+	+
8	1828.0			+	58	55,991		+	
9	2282.7		+	+					

Table 5. Selected eigenanalysis and basis selection results for an arch structure under 114.3 N/m loading.

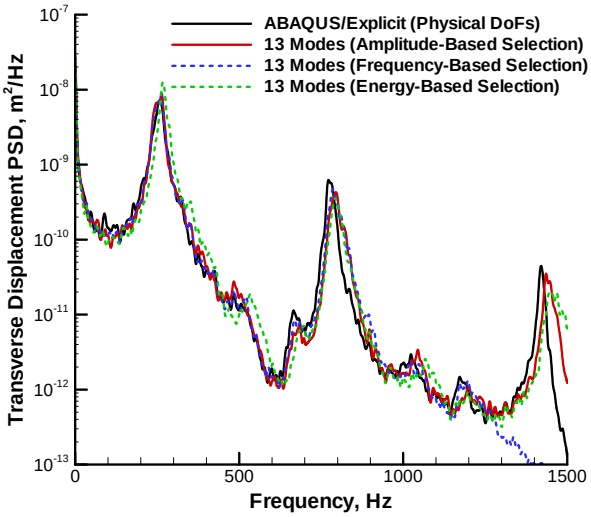

Figure 5. Transverse displacement PSD at the mid-span location.

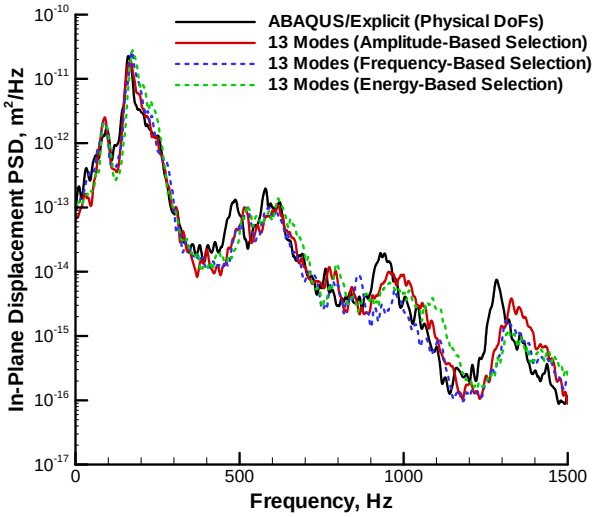

Figure 6. In-plane displacement PSD at the mid-span location.

3.3 Plate example

Finally, the two new modal basis selection procedures were applied to a substantially larger two-dimensional plate structure [9]. The plate dimensions were 0.3556 m by 0.2540 m with a thickness of 1.016 mm. The FE model was constructed using 8960 S4R four node elements, each measuring 3.175 mm by 3.175 mm. The S4R element features six DoFs per node, thus the plate model contained the total of 54,918 DoFs, or two orders of magnitude more than the beam or arch models. The plate was clamped on all four edges with all six DoFs constrained. Since the inclusion of the rotational DoF type did not significantly alter the result in the beam case, as evidenced in section 3.1.1.1, the plate procedure was based on the three translational DoF types only, i.e., one transverse and two in-plane.

The random acoustic load was modeled as truncated white noise with a cut-off frequency of 1024 Hz and OASPL of 154 dB. The total duration of the simulation used to perform system identification was 1.0 s, from which the initial transient of 0.5 s was removed to provide a developed response. With a sampling rate of 50 μs, 10,000 displacement and velocity snapshots were formed. The number of snapshots was lower than that used in the beam and arch cases because no instabilities (snap-through or auto-parametric response) were identified. Consequently, the simulation results presented are based on a shorter simulation time using a single 2.1384 s ensemble. When the initial transient of 0.5 s was removed, this left 1.6384 s of fully developed response. A 16,384-point FFT was used to compute the PSDs, giving a frequency resolution of 1.22 Hz. Based on the previous studies conducted with the MAP and the LNM expansion procedure using a coefficient cut-off of 0.5, 35 LNMs were found sufficient to accurately capture the plate response [9].

3.3.1 Plate example results

While the total set of LNMs included over 50,000 vectors, the POMs were projected only on a subset of the first 1279 LNMs present below 50 kHz. The results are summarized in Table 6.

Transverse LNMs					In-plane LNMs				
LNM Number	Frequency (Hz)	MAP (16T + 19I)	EPF (18T + 17I)	MEP (32T + 3I)	LNM Number	Frequency (Hz)	MAP (16T + 19I)	EPF (18T + 17I)	MEP (32T + 3I)
1	109.3	+	+	+	391	15,603	+	+	+
4	290.2	+	+	+	520	20,448	+	+	+
8	494.1	+	+	+	558	21,917	+	+	+
11	641.7	+	+	+	634	24,902	+	+	
12	657.7	+	+	+	708	27,912	+	+	
19	991.1	+	+	+	785	30,812	+	+	
22	1156.0	+	+	+	834	32,736	+	+	
23	1194.0	+	+	+	862	33,667	+	+	
28	1352.9	+	+	+	895	34,639	+	+	
30	1493.5	+	+	+	991	38,971	+		
35	1675.5	+	+	+	1012	39,515	+	+	
40	1833.3	+	+	+	1098	42,830	+	+	
46	2162.0	+	+	+	1099	42,945	+	+	
47	2165.9	+	+	+	1136	44,300	+		
48	2212.5	+	+	+	1173	45,876	+	+	
53	2369.4		+	+	1179	46,078	+	+	
59	2675.8	+	+	+	1206	47,085	+	+	
60	2686.2		+	+	1234	48,405	+	+	
62	2822.8			+	1257	49,158	+	+	
68	2999.5			+					
72	3166.4			+					
81	3557.6			+					
83	3649.4			+					
85	3686.9			+					
86	3712.9			+					
90	3812.9			+					
92	4005.8			+					
93	4025.7			+					
105	4498.8			+					
111	4647.0			+					
116	4870.4			+					

Table 6. Selected eigenanalysis and basis selection results for a plate structure under 154 dB loading.

It is seen that, consistent with the beam and arch examples, the MEP approach tends to favor more transverse and fewer in-plane LNMs in the basis compared to the other two approaches. The MAP and EPF approaches result in much similar sets of basis, consistent with the beam and arch examples. The bases identified by those two approaches differ only by four out of 35 LNMs.

Like the arch example, the results of the modal expansion (details not presented for brevity) indicate that POMs with low modal energy participation factors tend to decompose into more LNMs than those with higher participations. At the same time the low modal energy participation factor POMs tend to be dominated by the in-plane behavior.

Reduced-order simulation results obtained with the three selection procedures and full-order simulations are presented in Figure 7 and Figure 8 for transverse and in-plane displacements, respectively. It is seen that all three reduced-order solutions compare favorably with the full-order solution. While the MEP solution, with its basis heavily weighted with transverse LNMs, is somewhat better at capturing the transverse response (see third broad peak in Figure 7), it is less successful in capturing the in-plane response than the other two methods, see Figure 8. Hence, for a fixed modal basis size, there may be a trade-off between the number of transverse versus in-plane LNMs, and the accuracy of the transverse versus in-plane solutions.

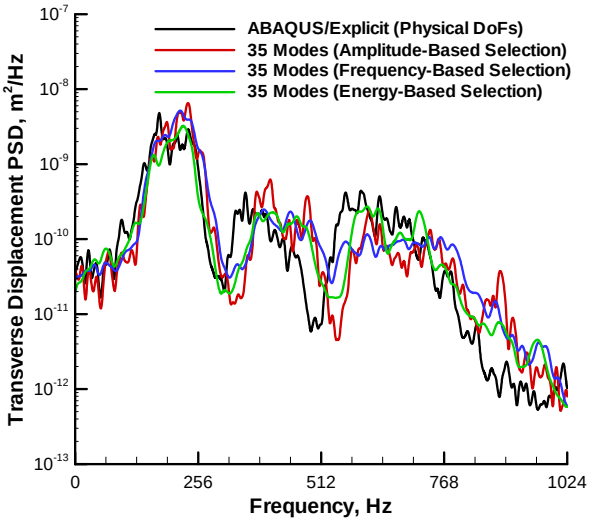

Figure 7. Transverse displacement PSD at the quarter-quarter span location.

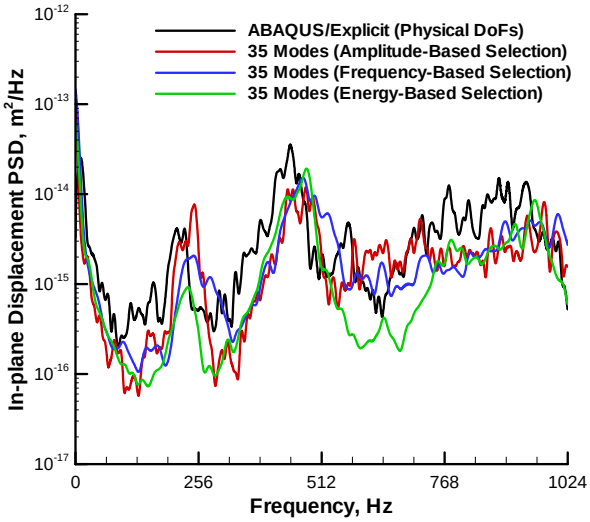

Figure 8. In-plane (in the shorter plane dimension) displacement PSD at the quarter-quarter span location.

4. CONCLUDING REMARKS

Three modal basis selection approaches were investigated and corresponding reduced-order analyses results were compared with a full-order simulation in physical DoFs. All three approaches yielded results which compared favorably with the full-order simulation. The previously developed MAP approach required only displacement response data for its system identification procedure and was based solely on POD analysis. The two new approaches, MEP and EPF, required both displacement and velocity response data for their system identification procedures and utilized both POD and SOD analyses. Therefore, the MAP approach required a smaller set of response data, but involved separation of DoFs types. The other two approaches allowed all DoF types simultaneously, but required a larger input data

set. The latter can be mitigated by obtaining the velocities through differentiating displacements, rather than acquiring and storing them explicitly, as was done in the present work.

For the cases considered, it was also found that the translational displacement data set produced modal bases comparable to those obtained when both translational and rotational DoF types were used in the MEP and EPF procedures. The EPF approach produced modal bases closely aligned with the MAP approach, i.e., relatively balanced between the number of transverse and in-plane LNMs, while the MEP approach tended to result in modal bases more heavily weighted with transverse LNMs than in-plane LNMs. Further investigation of the two new approaches is needed for mixed-element FE models, e.g. thin-walled panels with substructure, as well as for structures exhibiting stronger transverse to in-plane coupling, e.g. structures with greater curvature

REFERENCES

[1] Muravyov, A.A. and Rizzi, S.A., "Determination of nonlinear stiffness with application to random vibration of geometrically nonlinear structures," *Computers and Structures*, Vol. 81, No. 15, pp. 1513-1523, 2003.

[2] Mei, C., "Three decades' interesting experience in nonlinear finite element formulation development and aerospace applications," *Structural Dynamics: Recent Advances, Proceedings of the 8th International Conference*, The Institute of Sound and Vibration Research, University of Southampton, Paper No. 1, Southampton, UK, 2003.

[3] Hollkamp, J.J., Gordon, R.W., and Spottswood, S.M., "Nonlinear modal models for sonic fatigue response prediction: a comparison of methods," *Journal of Sound and Vibration*, Vol. 284, No. 3-5, pp. 1145-1163, 2005.

[4] Mignolet, M.P., Radu, A.G., and Gao, X., "Validation of reduced order modeling for the prediction of the response and fatigue life of panels subjected to thermo-acoustic effects," *Structural Dynamics: Recent Advances, Proceedings of the 8th International Conference*, The Institute of Sound and Vibration Research, University of Southampton, Paper No. 55, Southampton, UK, 2003.

[5] McEwan, M.I., Wright, J.R., Cooper, J.E., and Leung, Y.T., "A combined modal/finite element analysis technique for the dynamic response of a non-linear beam to harmonic excitation," *Journal of Sound and Vibration*, Vol. 243, No. 4, pp. 601-624, 2001.

[6] Dhainaut, J.M., Duan, B., Mei, C., Spottswood, S.M., and Wolfe, H.F., "Non-linear response of composite panels to random excitations at elevated temperatures," *Structural Dynamics: Recent Advances, Proceedings of the 7th International Conference*, Vol. 2, pp. 769-784, Southampton, England, 2000.

[7] Tiso, P., Jansen, E., and Abdalla, M., "A reduction method for finite element nonlinear dynamic analysis of shells," *Proceedings of the 47th AIAA/ASME/ASCE/AHS/ASC Structures, Structural Dynamics, and Materials Conference*, AIAA-2006-1746, Newport, RI, 2006.

[8] Guo, X., Lee, Y.Y., and Mei, C., "Nonlinear random response of laminated composite shallow shells using finite element method," *International Journal for Numerical Methods in Engineering*, Vol. 67, No. 10, pp. 1467-1489, 2006.

[9] Przekop, A. and Rizzi, S.A., "An efficient modal basis selection criteria for reduced-order nonlinear simulation," *Proceedings of the 7th European Conference on Structural Dynamics*, Paper E69, Southampton, UK, 2008.

[10] Przekop, A. and Rizzi, S.A., "Nonlinear reduced-order analysis with time-varying spatial loading distributions," *Journal of Aircraft*, Vol. 46, No. 4, pp. 1395-1402, 2009.

[11] Rizzi, S.A. and Przekop, A., "System identification-guided basis selection for reduced-order nonlinear response analysis," *Journal of Sound and Vibration*, Vol. 315, No. 3, pp. 467-485, 2008.

[12] Guo, X. and Przekop, A., "Energy-based modal basis selection procedure for reduced-order nonlinear simulation," *Proceedings of the 51st AIAA/ASME/ASCE/AHS/ASC Structures, Structural Dynamics, and Materials Conference*, AIAA-2010-2796, Orlando, FL, 2010.

[13] Chelidze, D. and Zhou, W., "Smooth orthogonal decomposition-based vibration mode identification," *Journal of Sound and Vibration*, Vol. 292, No. 3-5, pp. 461-473, 2006.

[14] Feeny, B.F. and Kappagantu, R., "On the physical interpretation of proper orthogonal modes in vibration," *Journal of Sound and Vibration*, Vol. 211, No. 4, pp. 607-616, 1998.

[15] Kumar, N. and Burton, T.D., "Use of random excitation to develop POD based reduced order models for nonlinear structural dynamics," *Proceedings of the ASME 2007 International Design Engineering Technical Conference and Information in Engineering Conference IDETC/CIE 2007*, DETC2007-35539, Las Vegas, NV, 2007.

[16] Farooq, U. and Feeny, B.F., "Smooth orthogonal decomposition for modal analysis of randomly excited systems," *Journal of Sound and Vibration*, Vol. 316, No. 1-5, pp. 137-146, 2008.

[17] Feeny, B.F. and Liang, Y., "Interpreting proper orthogonal modes of randomly excited vibration systems," *Journal of Sound and Vibration*, Vol. 265, No. 5, pp. 953-966, 2003.

[18] Rizzi, S.A. and Przekop, A., "Estimation of sonic fatigue by reduced-order finite element based analysis," *Structural Dynamics: Recent Advances, Proceedings of the 9th International Conference*, The Institute of Sound and Vibration Research, University of Southampton, Paper 129, Southampton, UK, July, 2006.

[19] *ABAQUS Online Documentation*. Providence, RI, Dassault Systemes Simulia Corp., 2009.

[20] Rizzi, S.A. and Muravyov, A.A., "Comparison of nonlinear random response using equivalent linearization and numerical simulation," *Structural Dynamics: Recent Advances, Proceedings of the 7th International Conference*, The Institute of Sound and Vibration Research, University of Southampton, Vol. 2, pp. 833-846, Southampton, UK, 2000.